23. Connell, J. H., Hughes, T. P. & Wallace, C. D. A 30-year study of coral community dynamics: influence of disturbance and recruitment on abundance, at several scales in space and time. *Ecol. Monogr.* **67,** 461–488 (1997).
24. Hughes, T. P. Demographic approaches to community dynamics: a coral reef example. *Ecology* **77,** 2256–2260 (1996).
25. Kojis, B. in *Proc. Colloquium on Global Aspects of Coral Reefs: Health, Hazards, History* (ed. R. N. Ginsburg) P35–P41 (Univ. Miami, Florida, 1993).
26. Connell, J. H. Disturbance and recovery of coral assemblages. *Coral Reefs* **16(Suppl.),** 101–113 (1997).

Acknowledgements. We thank the 41 graduate-student volunteers from James Cook University (JCU) who provided field assistance, and D. Ayre, J. Caley, P. Doherty and L. Smith for comments on the manuscript. Research was funded by grants to T.P.H. from the Australian Research Council. This is contribution no. 162 of the Coral Group at JCU.

Correspondence and requests for materials should be addressed to T.P.H. (e-mail: terry.hughes@jcu.edu.au).

Robust and optimal use of information in stereo vision

John Porrill*, John P. Frisby*, Wendy J. Adams* & David Buckley†

*Departments of *Psychology and †Ophthalmology and Orthoptics, University of Sheffield, Sheffield S10 2TN, UK*

Differences between the left and right eye's views of the world carry information about three-dimensional scene structure and about the position of the eyes in the head. The contemporary Bayesian approach to perception[1,2] implies that human performance in using this source of eye-position information can be analysed most usefully by comparison with the performance of a statistically optimal observer. Here we argue that the comparison observer should also be statistically robust, and we find that this requirement leads to qualitatively new behaviours. For example, when presented with a class of stereoscopic stimuli containing inconsistent information about eccentricity of gaze, estimates of this gaze parameter recorded from one robust ideal observer bifurcate at a critical value of stimulus inconsistency. We report an experiment in which human observers also show this phenomenon and we use the experimentally determined critical value to estimate the vertical acuity of the visual system. The Bayesian analysis also provides a highly reliable and biologically plausible algorithm that can recover eye positions even before the classic stereo-correspondence problem is solved, that is, before deciding which features in the left and right images are to be matched.

To be able to specify the observer that is statistically optimal for a perceptual task[3], a stochastic model of sensor noise must be available. For mathematical convenience, simple models, such as additive gaussian noise, are generally used. Although such models are adequate for describing some sources of error, most sensory data will also contain a proportion of rogue data items. It is reasonable to assume that perceptual systems have evolved to deal with this problem. We therefore introduce the idea of a robust ideal observer, that is, an observer that has optimal performance in the presence of a suitably specified population of outliers. We take this terminology from statistics, where the population mean is a simple example of a non-robust estimator and the median and mode of robust estimators. Robust and non-robust ideal observers will show quantitatively different levels of performance as the proportion of outliers increases. What is more interesting is that they can also show qualitatively different behaviour under certain experimental conditions, leading to a new type of comparison between ideal observer and human performance.

We have applied the robust ideal observer analysis to the following problem in stereo vision. The disparity in position between left and right retinal images of a point in the field of vision can be decomposed into horizontal and vertical components. The horizontal components H contain information about the three-dimensional structure of the world scene but they cannot be interpreted fully without knowledge of two viewing parameters that determine the positions of the eyes in the head: g, the gaze angle of the fixation point from the median plane of the head, and d, the distance to the fixation point. It is often more convenient to use the alternative dimensionless parameters[4] $\alpha = Ig/d$ and $\beta = I/d$, where I is the interocular separation. Because the vertical component of disparity V depends to first order on only these viewing parameters and not on visual scene depths, measurements of V can, in principle, be used to determine the viewing parameters and calibrate the information in H. We use the term V analysis to describe the recovery of viewing parameters from V measurements[5–10].

The experimental tool we used to investigate V analysis is the induced effect[11]. This is produced when one eye's view of a frontoparallel plane is magnified in the vertical dimension. The effect is a perceived rotation of the plane about a vertical axis through an angle that is approximately proportional to the applied magnification. The size of the effect in human observers is consistent with their performing V analysis to derive an incorrect eccentric gaze position and interpreting H information accordingly[6–10]. A convenient way to measure the induced effect is to have the observer vary a second magnification applied in the horizontal dimension which also produces a perceived slant about a vertical axis, an effect called the geometric effect. The horizontal magnification can be adjusted until the geometric and induced effects cancel and the surface appears frontoparallel.

Human and ideal observer performances were compared on this nulling task. The random-dot stimuli used were designed to probe the robustness of V analysis by using specified outlier populations. Half of the dots in the right image were given a vertical magnification m, selected from the range 0–12%, and the other half were given a vertical magnification $-m/2$ in the range 0–6%. As m increased, the two populations of points were therefore consistent with increasingly different viewing geometries.

Figure 1 shows Monte-Carlo simulations of the performance of a non-robust and a highly robust ideal observer on the nulling task. For an ideal observer, the nulling magnification required can be shown to equal its estimate of the viewing parameter α, so estimated α values from both observers are plotted against magnification m

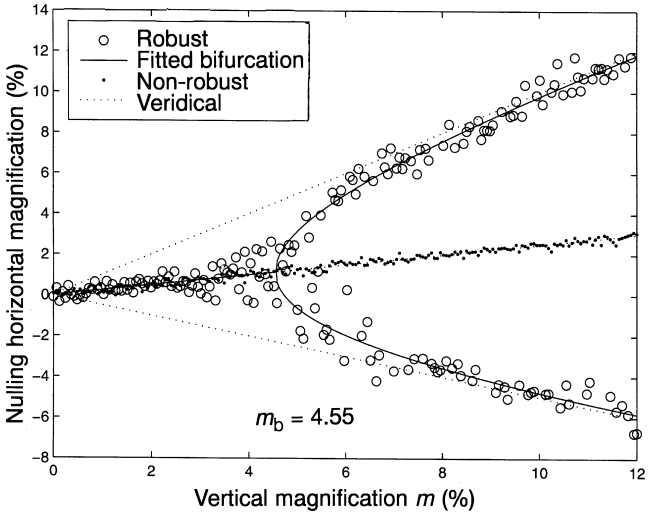

Figure 1 Monte-Carlo simulation of the performance of a non-robust and robust observer on the nulling task. The solid circles show the performance of the non-robust observer and the open circles show that of the highly robust ideal observer. The abscissa shows the range of m values used. The dotted lines show predicted induced effects m and $-m/2$ for single magnifications and for perfect pooling ($m/4$). The non-robust observer ($P = 1$, $k = 0.4°$) pools over the whole range, whereas the robust observer ($P = 0.001$, $k = 0.4$) shows initial pooling behaviour followed by a bifurcation. Values of P and k_{30} were chosen to match the observed value of m_b.

for each trial. The non-robust observer sets the nulling horizontal magnifications to the mean magnification over the two populations for the whole range of m values; we describe this behaviour as pooling[12,13]. In contrast, for the robust observer, initial pooling is followed by a bifurcation in which a magnification appropriate to one or other population is selected. Beyond a critical value of m, the robust observer in effect rejects one whole population as outliers and returns the viewing parameter appropriate to the other population. Which population is chosen is determined by statistical fluctuations.

Results for human observers are shown in Fig. 2 where the nulling magnifications recorded for each of four observers are plotted against m. As in the simulation, initial pooling is followed by a bifurcation at a critical magnification. A linear-hyperbolic bifurcation curve fitted the data significantly better than either a single straight line or two straight lines ($P < 0.001$ using a chi-squared statistic) and the fitted curve was used to estimate the critical magnification, m_b, which was found to be 4.4%. Consistent populations with magnifications of either m or $-m/2$ were also presented to the human observers. The group-mean settings for these stimuli are plotted with asterisks connected by lines. The two arms of the bifurcation for inconsistent data almost reach the curves for consistent populations. This indicates that human observers behave, at least qualitatively, like robust observers, and that data from one or other inconsistent population are successfully ignored for mixtures with large magnification differences. Note that the display appeared as a single planar entity throughout; observers did not report seeing two transparent planes at any time, as they do when populations with inconsistent H information are presented. This is consistent with the proposal that V is used to recover viewing parameters, which are intrinsically global in character. V is thus essentially different in character to H, which is a direct cue to shape and which is processed locally.

The measured critical value, m_b, offers the possibility of a quantitative comparison between human and robust ideal observer performance. To describe this comparison it is necessary to specify two aspects of the error model in more detail. First, acuity limitations were modelled as additive gaussian noise, the magnitude of which varied linearly with retinal eccentricity according to a model proposed in ref. 14. This model has a single free parameter, the acuity at a chosen eccentricity. As the effects of vertical disparity are generally wide-field phenomena, we quote values for k_{30}, the retinal vertical acuity at 30° eccentricity. Second, the proportion of outliers is given by $1 - P$, where P is the probability that a given left–right feature match is correct. At a given retinal position these outlier disparity measurements are distributed uniformly over the feasible matching range.

We plotted m_b values for robust ideal observers with different combinations of k_{30} and P (Fig. 3). Although the dependence on k_{30} is strong and nearly linear there is also some dependence on P (in fact bifurcation can be delayed arbitrarily by taking P close enough to 1). In the region in which the observer could realistically be called robust, that is $P < 99\%$, the observed bifurcation at $m_b = 4.4\%$ is consistent with k_{30} values between 0.2° and 0.4°. Assuming that the human observer is robust and close to ideal, this suggests a value for k_{30} of around 0.3°. This is consistent with horizontal-disparity acuity for single points and with the value assumed for vertical acuity in ref. 15. Because no direct measurement of vertical-disparity acuity has been reported we regard our approach as providing an independent estimate derived from a task chosen for its suitability for solution using vertical-disparity information.

The robust ideal observer for small P is optimized to deal with situations in which most of the data are incorrect. This is the case when vertical-disparity analysis occurs before match verification using all potential matches within the allowed vertical-matching range. Contrary to what one might expect, performance in recovering viewing parameters does not show any pronounced decline in this situation. A robust ideal observer can reliably recover α and β and the equivalent g and d parameters on a data set containing a large majority of incorrect matches (Fig. 4). This is important because, if viewing parameters can be recovered before the matching problem is solved, they can greatly simplify its subsequent solution by restricting the search for correct matches to those consistent with the prevailing viewing geometry. We speculate that robust estimators may be able to perform other stereoscopic tasks without previously solving the matching problem. This may help to explain why the human visual system can sometimes tolerate considerable perturbations in the vertical locations of corresponding points in the left and right images[16,17].

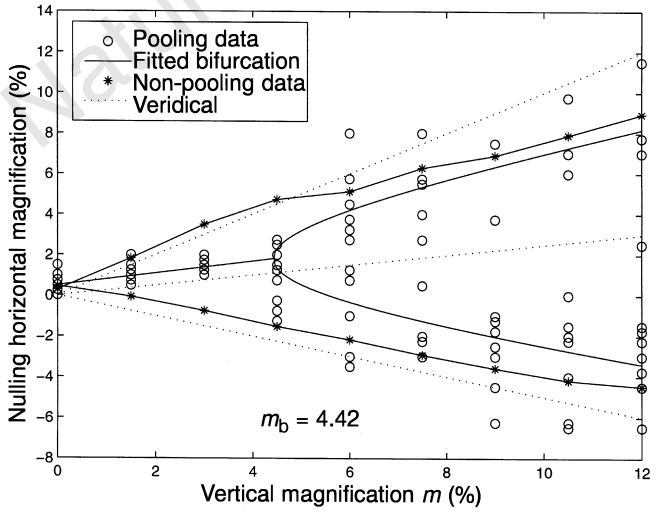

Figure 2 Pooling experiment where nulling magnifications for each of four observers are plotted against vertical magnification. The open circles show data for mixed magnification stimuli; they represent individual settings for each particular pairing of m and $-m/2$. The bifurcation from pooling behaviour is clearly visible. The best-fit linear-hyperbolic bifurcation curve ($m_b = 4.4\%$) is also shown. Asterisks connected by lines show group-mean data for consistent populations with vertical-image magnifications of either m (upper line) or $-m/2$ (lower line).

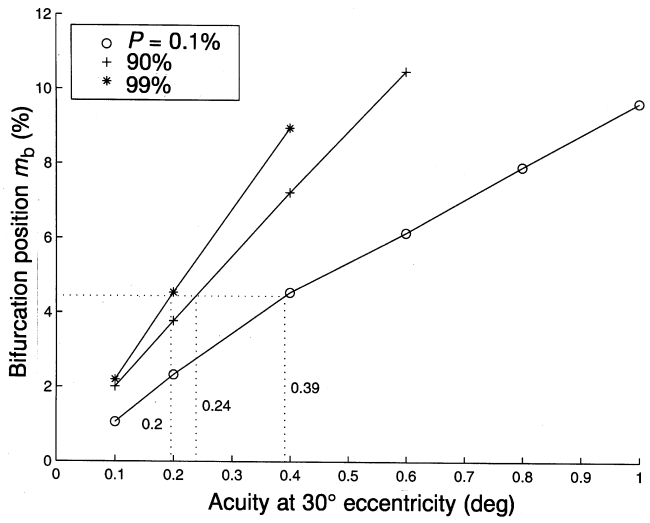

Figure 3 Bifurcation position versus acuity. The plotted curves show the predicted dependence of critical magnification on acuity k_{30} (abscissa) for three values of P, 0.1%, 90%, 99%, covering the range of 'robust' observers. The value of k_{30} giving the observed bifurcation position $m_b = 4.4\%$ is shown for each value of P.

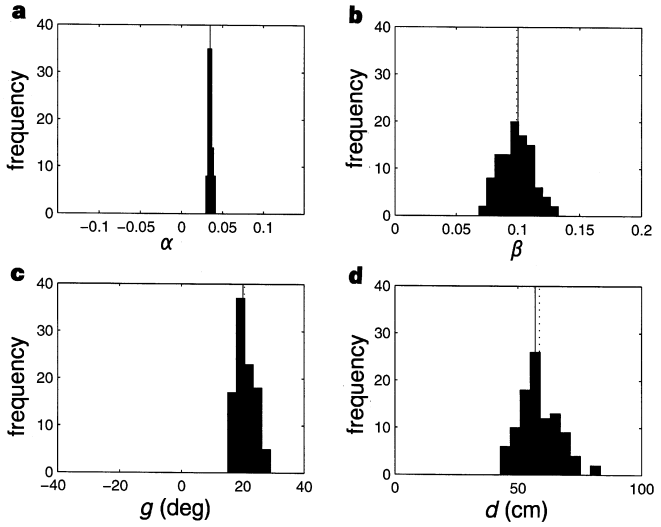

Figure 4 Performance of the robust ideal observer. The four graphs show histograms of 200 α and β values (**a** and **b** respectively) and the equivalent g and d values (**c** and **d** respectively) recovered by the robust ideal observer in the Hough limit ($P = 0.001$, $k = 0.4°$) for a 20-cm diameter, frontoparallel surface patch at a distance of 57 cm. For every correct match (512 in all) there were 10 incorrect matches distributed uniformly over the possible vertical matching range at that location. Dotted lines show the true parameter value and solid lines show the population mean. The simulation shows usable accuracy and small bias for all parameters, with particularly good recovery of α.

The limit of small P has a further useful property. In the limit as $P \rightarrow 0$ the robust ideal observer can be implemented using an efficient parameter-estimation algorithm which is often used in computer vision and which is called the Hough transform[18–20]. Hough algorithms are suitable for biological implementation as low-connectivity neural nets[21]. In our application, viewing-parameter pairs can be place-coded by a two-dimensional layer of neurons taking a weighted sum of inputs from disparity-selective binocular cells with which they are consistent. If these neuronal inputs measure the a-priori probability that a binocular feature has been correctly detected, the output will measure the posterior probability that the coded viewing parameters are correct. Winner-take-all competition in the output layer then estimates the optimal viewing parameters. Note that because this implementation codes probabilities, it is well adapted to the statistical combination of V information with viewing-parameter information from other sources (for example the oculomotor system).

We conclude by emphasizing three points. First, the psychophysical results show that human performance is well modelled by the robust ideal observer assumption, yielding a new method for estimating vertical-disparity acuity. Second, the analysis is based on the observation of a bifurcation onset rather than on a performance threshold. To our knowledge, an ideal observer analysis of human performance has not previously been based on a critical phenomenon of this kind. Third, we have derived a biologically plausible algorithm for vertical-disparity pooling which can recover accurate viewing-parameter estimates from noisy measurements of vertical disparity, including large numbers of incorrect matches. Thus the Bayesian approach, which would seem at first sight to offer information only about performance thresholds, can provide insights into perceptual systems at all three of the levels of understanding described in ref. 22: the computational (task description) level, the algorithmic (information representation and transformation) level and the implementation (physical realization or hardware) level. □

Methods

Experiment. Stereograms were presented on a Silicon Graphics Indy monitor using Crystal Eyes stereo glasses. A chin-rest, bite-bar and forehead bar kept observers' heads square to the screen and 57 cm from it. The room was completely dark. The edges of the monitor and the keyboard were covered with black card to exclude external sources of V information. The stimuli were roughly circular patches (diameters subtended about 21.5 cm) of 512 red dots (dot size <2 arcmin). Key-presses stepped horizontal magnification from –9 to 15% in steps of 0.25%, with a random starting magnification on each trial. Each observer produced three settings for each condition, collected from trials shown in randomized orders and distributed over three ~15-min sessions separated by breaks of at least 4 h. Each condition was seen for ~60 s to ensure that the induced effect had reached a steady state[23]. The four participants, one female and three males, were all experienced in psychophysical experiments. They were aged between 24 and 40 years and all had normal or corrected-to-normal vision and stereo acuity of 50 arcsec or better. Three participants (J.P., W.J.A. and D.B.) were authors; their data were not qualitatively different from those of the other observer.

Theory. The horizontal and vertical components of disparity of a point with retinal coordinates (x, y) and depth z relative to the fixation point in the local cyclopean frame are given to good accuracy by the linearized disparity equations of refs 7, 8:

$$H = \beta^2 \frac{z}{I} + \alpha x + \beta x^2$$

$$V = \alpha y + \beta xy$$

These equations can be extended to take account of the effects of eye elevation and cyclotorsion but we will not consider that refinement here[10]. Our hypothesis is that viewing parameters are recovered from V and used to recover scene structure z from H. Suppose that the true value of α is zero. Vertical magnification of the right image adds to V a term proportional to y, leading to a non-zero estimate for α. Allowing for the contribution of αx to H, the induced effect is generated. Horizontal magnification of the right image adds a term μx to H which exactly nulls this effect when $\mu = -\alpha$; hence the nulling task is a measurement of the viewing-system estimate of α.

If the correct viewing parameters are α and β, the vertical-disparity error on a match $M = (x, y, V)$ is $n = V - \alpha y - \beta xy$. The distribution of these errors is modelled as the sum of a uniform distribution due to incorrect matches plus a gaussian distribution representing acuity limitations:

$$p(n) = \frac{1-P}{\rho} + \frac{P}{\sigma\sqrt{2\pi}} \exp - \frac{n^2}{2\sigma^2} \propto 1 + q \exp - \frac{n^2}{2\sigma^2}$$

where $q = P/(1-P)(\rho/\sigma\sqrt{2\pi})$, ρ is the vertical matching range at that retinal position and σ is vertical-disparity acuity. Variation of σ with eccentricity E is modelled using the formula[14]

$$\sigma = \sqrt{2} k_0 (1 + 0.59E)$$

where k_0 is foveal acuity, E is measured in degrees and the factor of $\sqrt{2}$ accounts for addition of independent errors in the two eyes.

Using Bayes' theorem the probability density function $p(\alpha, \beta | M_1, \ldots, M_N)$ for the viewing parameters α and β, given the information in N matches, is

$$p(\alpha, \beta | M_1, \ldots, M_N) \propto \prod_I p(m_1 | \alpha, \beta) \propto \prod_i p(n_i) \propto \prod_i \left(1 + q_i \exp - \frac{n_i^2}{2\sigma_i^2}\right)$$

where we have assumed no previous knowledge and independence of match information. The ideal observer for α given the hit-or-miss[24] cost-function chooses α to maximize the marginal posterior density function

$$p(\alpha | M_1, \ldots, M_N) = \int p(\alpha, \beta | M_1, \ldots, M_N) \mathrm{d}\beta$$

Alternatively, the ideal observer for both α and β maximizes $p(\alpha, \beta | M_1, \ldots M_N)$. The second procedure was used in the simulations. Maximization was performed numerically over a fine grid of α, β values and refined by interpolation. In the limit $P \rightarrow 0$, all the q_i values are small and we can approximate the product above by

$$p(\alpha, \beta | M_1, \ldots, M_N) \propto 1 + \sum_i w_i q_i \quad \text{where} \quad w_i = \exp - \frac{n_i^2}{2\sigma_i^2}$$

Here each match makes an additive contribution q_i (which can be regarded as a measure of match goodness) weighted by its consistency w_i with a given α, β pairing. As the w_i values are small away from the line $\alpha x_i + \beta x_i y_i = V_i$ in α, β space, the algorithm reduces to a Hough transform[18,20,25] where each match makes a line of contributions into an accumulator array.

Received 1 June; accepted 3 November 1998.

1. Knill, D. C. & Richards, W. *Perception as Bayesian Inference* (Cambridge Univ. Press, Cambridge, 1996).
2. Adelson, E. H. & Weiss, Y. A simple Bayesian model predicts a complex set of phenomena. *Perception* **27 (Suppl.),** 18 (1980).
3. Barlow, H. The absolute efficiency of perceptual decisions. *Phil. Trans. R. Soc. Lond. B* **290,** 71–82 (1980).
4. Gårding, J., Porrill, J., Mayhew, J. E. W. & Frisby, J. P. Stereopsis, vertical disparity and relief transformations. *Vision Res.* **35,** 703–722 (1995).
5. Koenderink, J. J. & van Doorn, A. J. Geometry of binocular vision and a model for stereopsis. *Biol. Cybern.* **21,** 29–35 (1976).
6. Petrov, A. P. A geometrical explanation of the induced size effect. *Vision Res.* **20,** 409–416 (1980).
7. Mayhew, J. E. W. The interpretation of stereo-disparity information: the computation of surface orientation and depth. *Perception* **11,** 387–403 (1982).
8. Mayhew, J. E. W. & Longuet-Higgins, H. C. A computation model of binocular depth perception. *Nature* **297,** 376–379 (1982).
9. Frisby, J. P. An old illusion and a new theory of stereoscopic depth perception. *Nature* **307,** 592–593 (1984).
10. Porrill, J., Mayhew, J. E. W. & Frisby, J. P. in *Frontiers of Visual Science: Proceedings of the 1985 Symposium* 90–108 (National Academy Press, Washington DC, 1985).
11. Ogle, K. N. in *The Eye* Vol. 4 Part II (ed. Davson, H.) 209–417 (Academic, New York, 1962).
12. Stenton, P., Frisby, J. P. & Mayhew, J. E. W. Vertical disparity pooling and the induced effect. *Nature* **309,** 622–623 (1984).
13. Adams, W. *et al.* Pooling of vertical disparity information in the human visual system. *Perception* **25,** 165–176 (1996).
14. Drasdo, N. The neural representation of visual space. *Nature* **266,** 554–556 (1977).
15. van de Grind, W. A., Erkelens, C. J. & Laan, A. C. Binocular correspondence and visual direction. *Perception* **24,** 215–235 (1995).
16. Rogers, B. J. & Bradshaw, M. F. Does the visual system use the epipolar constraint for matching binocular images? *Invest. Opthalmol. Vis. Sci.* **37,** 684 (1996).
17. Stephenson, S. B. & Schor, C. M. Human stereo matching is not restricted to epipolar lines. *Vision Res.* **37,** 2717–2723 (1997).
18. Stephens, R. S. The probabilistic Hough transform. *Image Vision Comput.* **9,** 66–71 (1991).
19. Ballard, D. H. Generalising the Hough transform to detect arbitrary shapes. *Pattern Recog.* **13,** 111–122 (1981).
20. Peek, S., Mayhew, J. E. W. & Frisby, J. P. Obtaining viewing distance and angle of gaze from vertical disparities using a Hough-type accumulator. *Image Vision Comput.* **2,** 180–190 (1984).
21. Ballard, D. H. Cortical connections and parallel processing: structure and function. *Behav. Brain Sci.* **9,** 67–120 (1986).
22. Marr, D. *Vision* (Freeman, San Francisco, 1982).
23. Kaneko, H. & Howard, I. P. Spatial limitation of vertical-size disparity processing. *Vision Res.* **37,** 2871–2878 (1997).
24. Kay, S. M. *Fundamentals of Signal Processing—Estimation Theory* (Prentice Hall International, New Jersey, 1993).
25. Porrill, J. & Frisby, J. P. Computation of binocular eye position from vertical disparities with the use of probabilistic place coding. *Perception* **26,** 39 (1997).

Correspondence and requests for materials should be addressed to J.P.F.

The protein MAP-1B links $GABA_C$ receptors to the cytoskeleton at retinal synapses

Jonathan G. Hanley, Peter Koulen*, Fiona Bedford, Phillip R. Gordon-Weeks† & Stephen J. Moss

MRC Laboratory for Molecular Cell Biology and Department of Pharmacology, University College, Gower Street, London WC1E 6BT, UK
** Max-Plank-Institut fur Hirnforschung, Neuroanatomische Abteilung, Deutschordenstrasse 46, 60528 Frankfurt, Germany*
† Developmental Biology Research Centre, Division of Biomedical Sciences, Kings College London, 26–29 Dury Lane, London WC2B 5RL, UK

The ionotropic type-A and type-C receptors for the neurotransmitter γ-aminobutyric acid ($GABA_A$ and $GABA_C$ receptors) are the principal sites of fast synaptic inhibition in the central nervous system[1–3], but it is not known how these receptors are localized at GABA-dependent synapses. $GABA_C$ receptors, which are composed of ρ-subunits[3–6], are expressed almost exclusively in the retina of adult vertebrates, where they are enriched on bipolar cell axon terminals[7–9]. Here we show that the microtubule-associated protein 1B (MAP-1B) specifically interacts with the $GABA_C$ ρ1 subunit but not with $GABA_A$ receptor subunits. Furthermore, $GABA_C$ receptors and MAP-1B co-localize at post-synaptic sites on bipolar cell axon terminals. Co-expression of MAP-1B and the ρ1 subunit in COS cells results in a dramatic redistribution of the ρ1 subunit. Our observations suggest a novel mechanism for localizing ionotropic GABA receptors to synaptic sites. This mechanism, which is specific for $GABA_C$ but not $GABA_A$ receptors, may allow these receptor subtypes, which have distinct physiological and pharmacological properties, to be differentially localized at inhibitory synapses.

To investigate the mechanisms responsible for the localization of ionotropic GABA receptors in neurons, we used a yeast two-hybrid screen[10]. We focused on $GABA_C$ receptors, which are composed of ρ(1–3) (ref. 3) subunits, unlike the more structurally diverse $GABA_A$ receptors, which are assembled from five subunit classes: α(1–6), β(1–4), γ(1–4), δ and ϵ (refs 1, 2). A retinal complementary DNA library was screened with a bait encoding the large intracellular domain of the $GABA_C$-receptor ρ1 subunit[1–3]. One of the strongly interacting clones, clone 8 (Fig. 1), corresponds to amino acids 460–690 of MAP-1B, which is 95% identical to this portion of the human protein (Fig. 1b)[11–14]. This interaction must be specific to the ρ1 subunit as clone 8 does not interact with the intracellular domains of selected $GABA_A$-receptor subunits[1,2], nor with that of the $GABA_C$-receptor ρ2 subunit[6] (Fig. 1a). These constructs all produced fusion proteins with Gal-4 in yeast of the expected sizes (relative molecular masses (M_r) were determined by western blotting; data not shown). To pinpoint the binding site for the ρ1 subunit on MAP-1B, smaller sections of clone 8 were tested for their interaction in yeast. Binding of the ρ1 subunit was critically dependent on amino-acid residues 460–565, but independent of the putative microtubule-binding domain within clone 8 (Fig. 1c)[11–14]. The interaction between clone 8 and the intracellular domain of the ρ1 subunit was confirmed by expressing both proteins as glutathione-*S*-transferase (GST) fusions[15]. Gel-overlay assay indicated that GST–ρ1 binds to GST–clone 8 but not to GST alone (Fig. 1d).

We analysed the interaction between the ρ1 subunit and MAP-1B

a

Bait	Growth on -His/ -Trp/-Leu	β-gal activity
ρ1	+	+
ρ2	–	–
α1	–	–
α2	–	–
γ2	–	–
β3	–	–

c

Truncation	Growth on -His/ -Trp/-Leu	β-gal activity
$8^{460\text{-}634}$	+++	+++
$8^{634\text{-}690}$	–	– – –
$8^{460\text{-}565}$	+++	+++

b

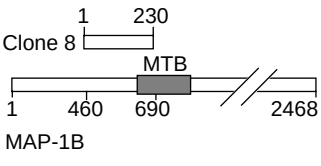

d

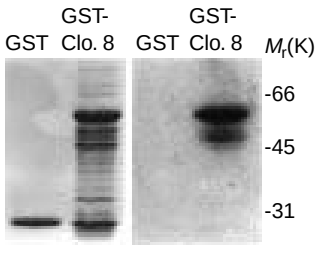

Figure 1 Specific interaction of the ρ1 intracellular domain with an N-terminal domain of MAP-1B. **a**, Interaction of clone 8 and the intracellular domain of the ρ1 subunit in yeast, as measured by growth on -His/-Trp/-Leu medium and β-galactosidase activity. **b**, Clone 8 encodes amino acids 460–690 of MAP-1B. **c**, The domain in MAP-1B responsible for binding ρ1, as determined by deletion analysis in yeast; interaction was measured as for **a**. **d**, ^{32}P-labelled GST–ρ1 interacts with GST–clone 8 (clo.8) in an overlay assay. Right, autoradiography; left, identical gel stained with Coomassie brilliant blue.